Structure of the Lowermost Mantle and the CMB West of Tonga- Fiji

Sebastian Rost
(srost@es.ucsc.edu)

Justin Revenaugh

Introduction

The surface and the core-mantle boundary (CMB) are the Earth's two most significant boundary layers. These boundaries presumably have the richest thermal, chemical and dynamic behavior of the planet.

To better understand the structure of the Earth's deep interior, we are studying the structure of the lowermost mantle, uppermost outer core and the core-mantle boundary in the region between Tonga-Fiji and Australia. We use earthquakes from the Tonga-Fiji region recorded at the 24-station, short-period, small aperture Warramunga array (WRA) in the Northern Territory, Australia. The dataset consists of approximately 370 events which cluster geographically into three separated groups. We are conducting a survey of the core-reflected phase ScP (**Fig. 1**) in the short-period data to resolve the small scale structure of the CMB. When the CMB shows discontinuity additional onsets in the seismogram are generated (**Fig. 1** and **Fig. 2**). We use ScP waveform modeling to resolve the structure at the CMB.

The dataset shows variations on different scale-lengths. The three event clusters (**Fig. 3**) show very different ScP to P amplitude ratios (**Fig. 4**). Source and receiver side structure can be ruled out as the sole cause of these differences. The varying amplitudes in the three clusters likely indicate small scale variations of the conversion conditions at the CMB in this region.

The high amplitude ScP phases in the south cluster (**Fig. 5**) are ideally suited for waveform modeling. Due to the high ScP amplitudes and the use of array recordings a modeling of single events is possible.

The waveform modeling indicates very different CMB structures in this region west of Tonga-Fiji. We are able to model IASP91-like CMB patches, Ultra-Low-Velocity-Zone structures above the CMB (**Figs. 6 - 9**) and Core-Mantle-Zone structures (**Figs. 10 & 12**) in some small regions (**Fig. 11**).

Method

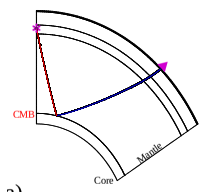

Figure 1: Cartoon of ray paths through the Earth's mantle. a) ScP ray path. b) Variation of ScP ray path when CMB structure is present. The ScP waveform is influenced by structure above the CMB (Ultra-Low-Velocity-Layer → ULVZ) and by structure below the CMB (Core-Mantle-Zone → CRZ).

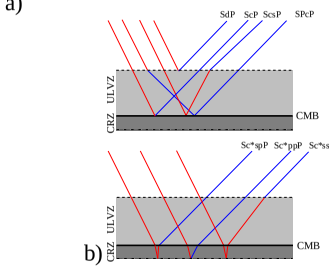

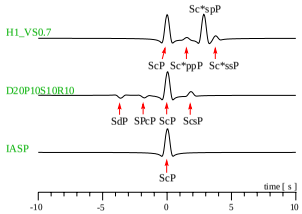

Figure 2: Synthetic Gaussian-beam seismograms for different CMB models. A IASP-like CMB produces one onset (ScP) in the seismogram. A ULVZ structure produces two precursors (SdP and SPcP) and one postcursor (ScsP) to ScP. A CRZ produces postcursors. The most important cores are Sc*spP, Sc*ppP, Sc*ssP with different travel times and amplitudes.

Data

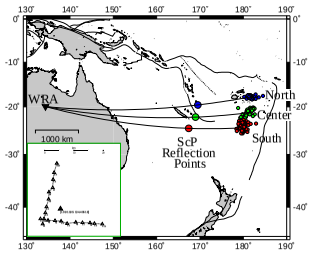

Figure 3: Source-receiver combination used for the study. We use events in the Tonga-Fiji region (lat=0/-60; long=150/190) recorded at the Warramunga Array (WRA) in Australia (inverted triangle). The sources cluster geographically into three separated groups as indicated by the colors of the sources. The large circles indicate the ScP-to-P conversion points at the CMB. The great circle paths are indicated by the black lines. The insert shows the WRA configuration with an aperture of ~20 km and 24 vertical stations.

The data was recorded from 1979 to 1984. The selected events are deeper than 300 km with distances of $\Delta \approx 40° - 44°$ and magnitudes of $m_b = 4.5 - 6.0$.

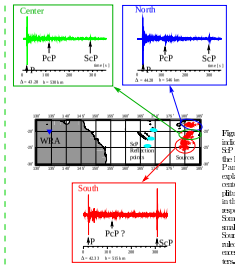

Figure 4: The three source clusters as indicated in **Fig. 3**. show very different ScP amplitudes. The south cluster shows the highest ScP amplitudes with ScP-to-P amplitudes of 0.4 - 0.7 which cannot be explained with a IASP-like model. The center and north cluster show nearly amplitudes consistent with IASP. The traces in this figure are WRA beam traces with respect to ScP. The onsets are marked. Since of the south cluster events show very small PcP amplitudes.

Source or receiver side structure can be ruled out as the sole cause of the differences of ScP amplitudes in the three clusters.

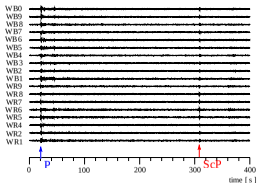

Figure 5: Seismogram example of event 18-NOV-1979U7238 (south cluster). The event was at a depth of h = 515 km, at a distance to WRA of $\Delta = 42.3°$. The fundamentals to WRA is $\Theta = 104.0°$ and the magnitude $m_b = 5.1$. The P and ScP onsets are marked.

ULVZ

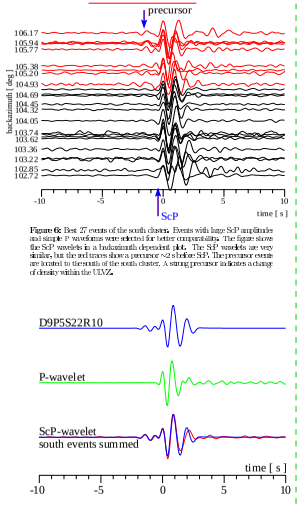

Figure 6: Best 27 events of the south cluster. Events with large ScP amplitudes and simple P waveforms were selected for better comparability. The figure shows the ScP wavelets in a back-azimuth dependent plot. The ScP wavelets are very similar, but the red traces show a precursor ~2 s before ScP. The precursor events are located to the north of the south cluster. A strong precursor indicates a change of density within the ULVZ.

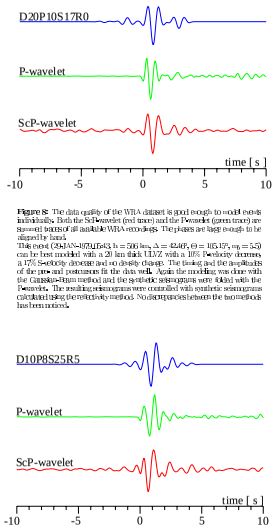

Figure 8: The data quality of the WRA dataset is good enough to model events individually. Both the ScP-wavelet (red trace) and the P-wavelet (green trace) are summed traces of all available WRA recordings. The phases are high enough to be aligned by hand.

This event (24-JAN-1979U7643) h = 506 km, $\Delta = 42.40°$, $\Theta = 105.15°$, $m_b = 5.5$) can be best modeled with a 20 km thick ULVZ with a 10% P-velocity decrease, a 17% S-velocity decrease and no density change. The fit of the fundamentals of the pre- and postcursors fit the data well. Again the modeling was done with the Gaussian-Beam method and the synthetic seismograms were filtered with the P-wavelet. The resulting seismograms were normalized with synthetic seismograms calculated using the reflectivity method. No discrepancies between the two methods has been noticed.

Figure 7: Waveform modeling of southernmost precursor events in **Fig. 6**. The red trace shows the summed precursor events shown as red lines in **Fig. 6**. The green line is the summed P wavelet of the same event. The ScP wavelet shows a precursor and perhaps a postcursor. The blue trace is the best fitting model of our modeling and is also overlaid over the ScP wavelet. The synthetic seismograms are calculated with the Gaussian-Beam method. The resulting seismograms are then folded with the P-wavelet to get a comparable seismogram. The model fit is satisfying, although the postcursor amplitude of the model is too large. The best-fitting model shows a 9 km thick ULVZ with a 5% P-velocity decrease, a 22% S-velocity decrease and a 10% density increase.

Figure 9: Waveform modeling for another event (03-MAY-1981J2483) h = 437 km, $\Delta = 42.05°$, $\Theta = 105.40°$, $m_b = 5.0$). The ScP-wavelet is best modeled with 10 km thick ULVZ which shows a 8% P-velocity decrease, a 25% S-velocity decrease and a small 5% density increase. The model differs strongly from the model shown in **Fig. 8**, indicating that the ULVZ structure changes on very small scale lengths.

CRZ

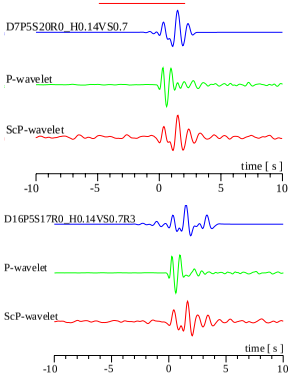

Figure 10: Some ScP waveforms cannot be modeled with a simple CMB or with a ULVZ like those shown in **Figs. 8 & 9**. Two of these events (24-NOV-1979U1928, h = 500 km, $\Delta = 42.03°$, $\Theta = 104.41°$, $m_b = 5.6$; 03-NOV-1981J2231, h = 505 km, $\Delta = 42.02°$, $\Theta = 105.32°$, $m_b = 5.0$) are shown here. These events show very deformed waveforms relative to the original P-wavelet. The events are best modeled with structures at the core side of the CMB and are consistent with a Core-Mantle-Zone. The CRZ is very thin (0.05 - 0.2 km) with S-velocities of 0.7 - 0.8 km/s and perhaps a small density decrease of 10% relative to the normal core material. Due to the thin zone the P-velocity in the CRZ cannot be constrained by analyzing ScP.

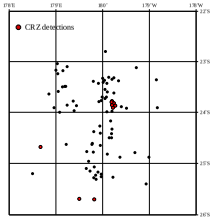

Figure 11: CRZ detections in the south cluster. All events showing good ScP waveforms are shown as black circles. The CRZ detections are shown as red circles. The CRZ detections are grouped in 3 groups. The biggest group consists of 6 events. No more evidence for CRZs have been detected in this dataset.

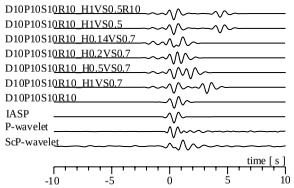

Figure 12: Gaussian-Beam synthetic seismograms for different CRZ models. CRZ models like those Figs. 4,12 too show different final flows which are too large to explain the data. The amplitude of the CRZ postcursors is sensitive to the density in the CRZ and the S-velocity. The Gaussian-Beam seismograms are compared with reflectivity synthetic seismograms and no differences have been found.

Conclusions

This study shows that short-period array recordings are perfect to study the small-scale structure at the CMB. The Tonga-Fiji dataset shows strong variations of ScP amplitudes which can be related to structures at the CMB. The ScP waveforms vary over very short scale lengths (< 50 km). Different structures at the CMB have been detected including simple (IASP-like) CMB, ULVZ and CRZ.

The ULVZ models show strong variations thickness, velocities and density. The CRZ models show thicknesses of 0.05 - 0.2 km with S-velocities of 0.7 - 0.8 km/s and perhaps a small density decrease of 5%. Other models of the CMB fail to explain the waveform data for the CRZ events. The CRZ detections are located in very small regions which are in agreement with the sedimentation of lighter material (core-mantle reaction products or "sediments?") in a topographic high of the CMB.